

Room-Temperature Vapor Deposition of Cobalt Nitride Nanofilms for Mesoscopic and Perovskite Solar Cells

Jin Soo Kang, Jae-Yup Kim, Jungjin Yoon, Jin Kim, Jiwoong Yang, Dong Young Chung,
Min-cheol Kim, Hansol Jeong, Yoon Jun Son, Bong Gyu Kim, Juwon Jeong,
Taeghwan Hyeon, Mansoo Choi,* Min Jae Ko,* and Yung-Eun Sung*

Organic/inorganic hybrid solar cells, typically mesoscopic and perovskite solar cells, are regarded as promising candidates to replace conventional silicon or thin film photovoltaics. There have been intensive investigations on the development of advanced materials for improved power conversion efficiencies, however, economical feasibilities and reliabilities of the organic/inorganic photovoltaics are yet to reach at a sufficient level for practical utilizations. In this study, cobalt nitride (CoN) nanofilms prepared by room-temperature vapor deposition in an inert N₂ atmosphere, which is a facile and highly reproducible procedure, are proposed as a low-cost counter electrode in mesoscopic dye-sensitized solar cells (DSCs) and a hole transport material in inverted planar perovskite solar cells (PSCs) for the first time. The CoN film successfully replaces conventional Pt in DSCs, resulting in a power conversion efficiency comparable to the ones based on Pt. In addition, PSCs employing the CoN manifest high efficiency even up to 15.0%, which is comparable to state-of-the-art performance in the cases of PSCs employing inorganic hole transporters. Furthermore, flexible solar cell applications of the CoN are performed in both mesoscopic and perovskite solar cells, verifying the advantages of the room-temperature deposition process and feasibilities of the CoN nanofilms in various fields.

1. Introduction

Organic/inorganic hybrid solar cells, whose performance has been rapidly enhanced recently, are regarded as promising devices for highly efficient and economical utilization of solar energy.^[1–4] Among them, mesoscopic solar cells, namely, dye-sensitized solar cells (DSCs), have received great attention due to their reliable performance and aesthetically favorable features,^[5–8] in addition to the unrivaled photon utilization under ambient light conditions (e.g., indoor applications).^[9] Meanwhile, perovskite solar cells (PSCs) exhibited unprecedented growth in power conversion efficiency, with a record certified efficiency of 22.1% in standard AM 1.5G condition.^[10–15] Recently, there have been significant advances in performance and technological viability due to incorporations of advanced materials and processes.^[16–26] However, the organic/inorganic hybrid solar cells are yet to meet the sufficient level required for their practical applications, particularly in terms of economic feasibility and long-term stability.^[27]

Dr. J. S. Kang, J. Kim, Dr. J. Yang, Dr. D. Y. Chung, Y. J. Son, B. G. Kim,
J. Jeong, Prof. T. Hyeon, Prof. Y.-E. Sung

Center for Nanoparticle Research
Institute for Basic Science (IBS)
Seoul 08826, Republic of Korea
E-mail: ysung@snu.ac.kr

Dr. J. S. Kang, J. Kim, Dr. J. Yang, Dr. D. Y. Chung, Y. J. Son, B. G. Kim,
J. Jeong, Prof. T. Hyeon, Prof. Y.-E. Sung

School of Chemical and Biological Engineering and Institute of
Chemical Processes (ICP)
Seoul National University
Seoul 08826, Republic of Korea

Prof. J.-Y. Kim
Division of Chemical Engineering
Hoseo University
Asan 31499, Republic of Korea

J. Yoon, M.-c. Kim, Prof. M. Choi

Global Frontier Center for Multiscale Energy Systems and Department of
Mechanical and Aerospace Engineering
Seoul National University
Seoul 08826, Republic of Korea
E-mail: mchoi@snu.ac.kr

H. Jeong

Photo-electronic Hybrids Research Center
Korea Institute of Science and Technology (KIST)
Seoul 02792, Republic of Korea

Prof. M. J. Ko

Department of Chemical Engineering
Hanyang University
Seoul 04763, Republic of Korea
E-mail: mjko@hanyang.ac.kr

 The ORCID identification number(s) for the author(s) of this article
can be found under <https://doi.org/10.1002/aenm.201703114>.

DOI: 10.1002/aenm.201703114

During the operations of organic/inorganic photovoltaics, extraction and collection of charge carriers from the light absorber to the external circuit are essential steps for solar-to-electrical energy conversion. Unfortunately, materials used for regeneration of light absorbers or carrier transport are causing cost issues in hybrid solar cells. In DSCs, Pt in counter electrodes is responsible for a large portion of manufacturing costs.^[28,29] Though various carbonaceous materials and conducting polymers in place of Pt exhibited comparable performance, they often suffer from insufficient stability.^[30,31] Meanwhile, state-of-the-art organic hole transport materials used in PSCs are either costly or unfavorable for long-term operations.^[32,33] In order to obtain economical feasibilities and reliable performance, various inorganic materials have been introduced in DSCs and PSCs as counter electrodes and hole transport materials, respectively. Transition metal compounds with nano-architectures (i.e., large surface area) have shown Pt-like performance in DSCs,^[34–45] and Cu compounds such as CuI^[46] and CuSCN^[47–49] and a number of oxides^[50–53] and sulfides^[54,55] manifested decent performance in PSCs. However, previously suggested approaches often require complicated synthesis and deposition processes and bring about damages to the light absorbers.^[32] Therefore, further improvements are necessary to utilize the inorganic materials in the hybrid solar cells in the aspect of practical usage.

Among low-cost inorganic materials, transition metal nitrides have received tremendous interest due to their favorable characteristics such as high conductivity and electrocatalytic activity (i.e., low charge transfer resistance) originated from metal-like properties and electronic structures resembling that of Pt, respectively.^[56–60] In addition, nitride materials have excellent chemical stability and corrosion resistance, which enable wide range of applications.^[57–63] However, conventional procedures for the synthesis of nitride materials often involve high-temperature heat treatment in toxic NH₃ atmosphere,^[37–39] and this method has limitation in synthesizing nitrides with high

N content, which is favorable for rapid charge transfer. Contrary to the previous approaches, we herein prepared cobalt nitride (CoN) nanofilms by room-temperature vapor deposition, and the CoN films were utilized as an electrocatalytic counter electrode in DSCs and a hole transport layer (HTL) in PSCs, for the first time according to the best of our knowledge. Though the deposition of the CoN film was performed in an inert N₂-filled chamber without an elevation of temperature, complete nitridation of Co to CoN during the deposition process was clearly verified by keen physicochemical characterization techniques. In addition, the CoN films had favorable structural characteristics for efficient electrocatalysis in DSCs and uniform deposition of perovskite light absorbers in PSCs. The CoN film in DSCs resulted in a high photovoltaic performance comparable to conventional Pt-based cells, and the CoN HTL led to the power conversion efficiency up to 15.0% in PSCs, which is comparable to the state-of-the-art performance among the PSCs employing inorganic hole transporters. Moreover, feasibility of the CoN film for flexible solar cell applications was investigated in both types of photovoltaics, demonstrating the advantage of the room-temperature preparation method and wide applicability of the CoN nanofilms.

2. Results and Discussion

2.1. Preparation and Characterization of the Cobalt Nitride Nanofilms

As described in a schematic image displayed in **Figure 1**, room-temperature vapor deposition of the CoN nanofilm was carried out by radio frequency (RF) sputtering of Co onto transparent conducting oxide (TCO) substrates in an inert N₂-filled chamber. For comparisons, Co films were also prepared by the identical method except for the usage of Ar instead of N₂. **Figure 2a** shows the X-ray diffraction (XRD) patterns of the Co and CoN

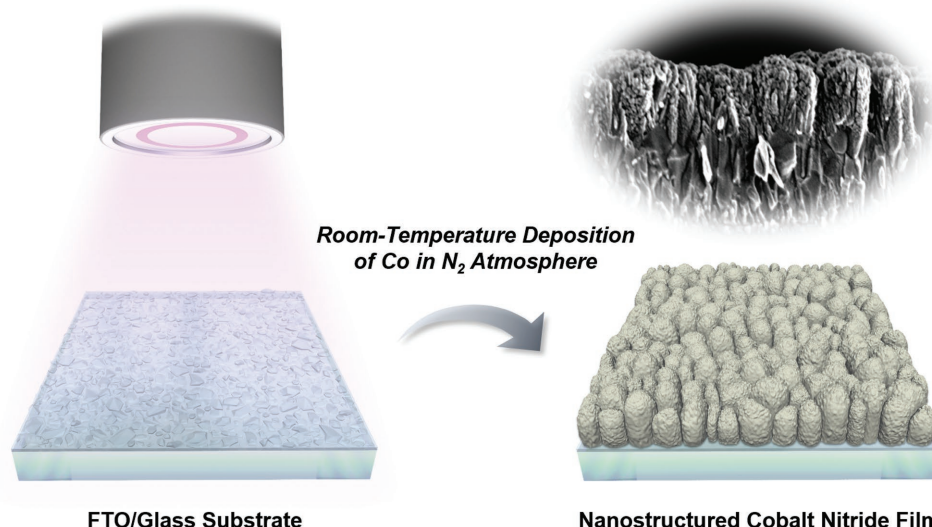


Figure 1. Preparation of the CoN nanofilms. Schematic images illustrating the preparation of the CoN nanofilm by room-temperature vapor deposition of cobalt in an inert N₂ atmosphere.

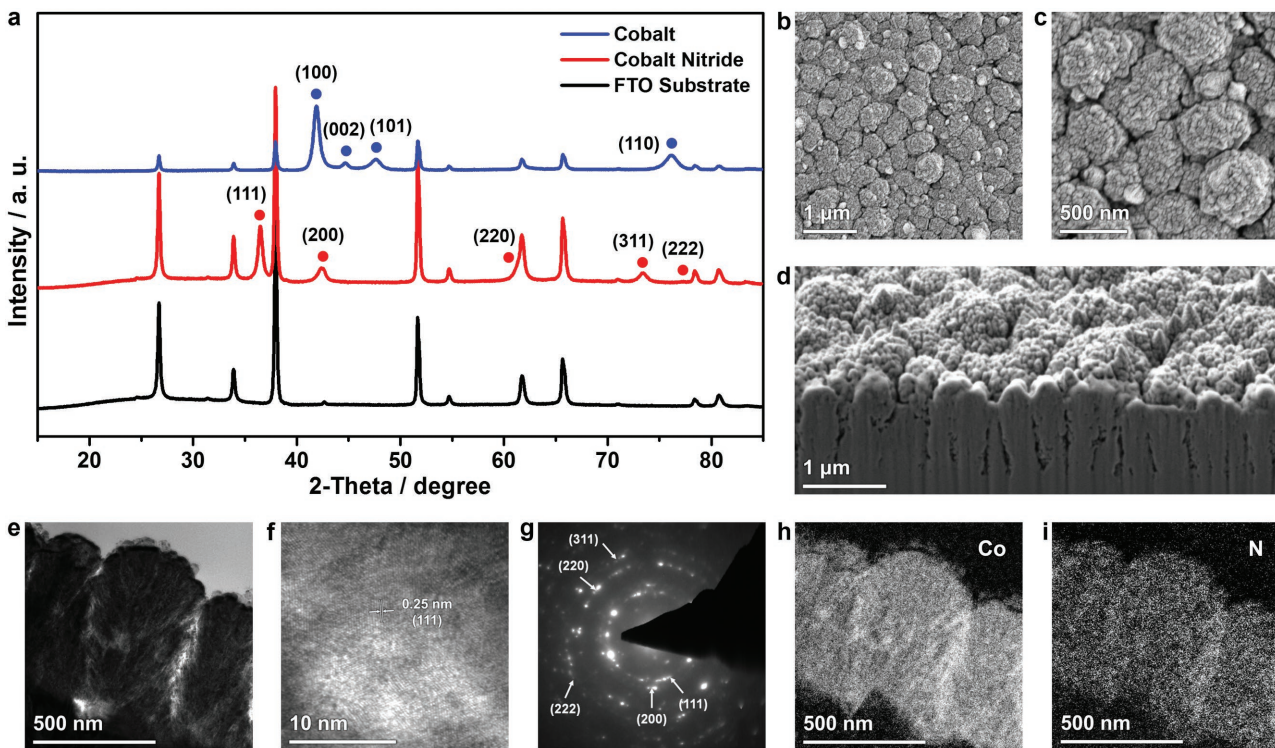


Figure 2. Materials characterizations. a) The XRD spectra of the Co and the CoN films deposited on FTO/glass substrates. The signals were assigned according to JCPDS 05-0727 (Co) and JCPDS 16-0116 (CoN). b,c) Top-view and d) cross-sectional SEM images of the CoN film. e) Low-magnification and f) high-magnification TEM images of the CoN film imaged after the preparation of a specimen with the assistance of FIB. g) SAED patterns and h,i) elemental EF-TEM maps of the CoN film.

films deposited on fluorine-doped tin oxide (FTO) coated glass, and nitridation of Co to CoN (with zinc blende structure) during the reactive sputtering was clearly verified. Figure 2b,c shows the top-view scanning electron microscope (SEM) images of the CoN film, where nanostructures with rough surfaces are clearly observable. For further understandings on the morphology, cross-sectional SEM images were obtained with the assistance of focused ion beam (FIB) milling. As can be seen from the SEM image displayed in Figure 2d, the CoN film had cauliflower-like structure of which height is around 600 nm. The nanomorphology of the CoN film was additionally analyzed by transmission electron microscope (TEM), and the TEM image (Figure 2e) shows dendritic nanostructure that matches well with the SEM images (Figure 2d and Figure S1, Supporting Information) was observed. From the high-magnification image in Figure 2f, we could observe lattice spacing of 0.25 nm, which corresponds to the *d*-spacing of (111) plane of CoN, and the selected area electron diffraction (SAED) pattern displayed in Figure 2g verified that the reactively sputtered CoN is polycrystalline. Moreover, elemental energy filtered (EF)-TEM maps (Figure 2h,i) show the uniform distribution of Co and N, indicating the effectiveness of our nitridation process.

Figure 3a–c shows the X-ray photoelectron spectroscopy (XPS) spectra of the Co and CoN deposited on the FTO substrates. All of the XPS signals were corrected based on the peak position of C 1s spectra (284.6 eV). From the survey spectra (Figure 3a), the presence of Co is clear in both samples, and the O peak from the CoN film implies that surface oxidation takes

place possibly due to the contact with oxygen in air. Figure 3b shows core level Co 2p spectra, and the binding energy positions of the peaks were compared with the previous reports. In the case of the Co film, peaks at 778.2 and 793.0 eV show the presence of Co–Co bond, and signals located at the binding energy positions of 780.8 and 796.2 eV are resulted from Co–O, implying that the significant portion of the Co film's surface was oxidized into Co_3O_4 considering the peak positions.^[64–66] In contrast, the CoN film manifested Co 2p peaks at 778.7 and 793.7 eV, which indicates that the oxidation state of Co in the CoN film is in between those of metallic Co and Co oxide. Therefore, together with the strong N 1s peak at 396.7 eV shown in Figure 3c, it could be concluded from the XPS results that the formation of Co–N bond took place during the reactive vapor deposition process.

Further characterizations on the oxidation states and coordination environments were carried out by synchrotron X-ray absorption fine structure (XAFS) analyses. Figure 3d shows the X-ray absorption near edge structure (XANES) spectra of the Co and CoN films obtained at Co K-edge. The CoN manifested significant increase in white line intensity and high-energy shift in absorption edge position as compared with the case of the bare Co film. Since XANES analysis provides information on the bulk property of the samples, it could be verified that the nitridation was complete in the CoN film. In addition, a noteworthy observation was made that the clear pre-edge in the CoN indicates that the Co atom has tetrahedral symmetry, and this result matched well with the zinc blende crystal structure verified

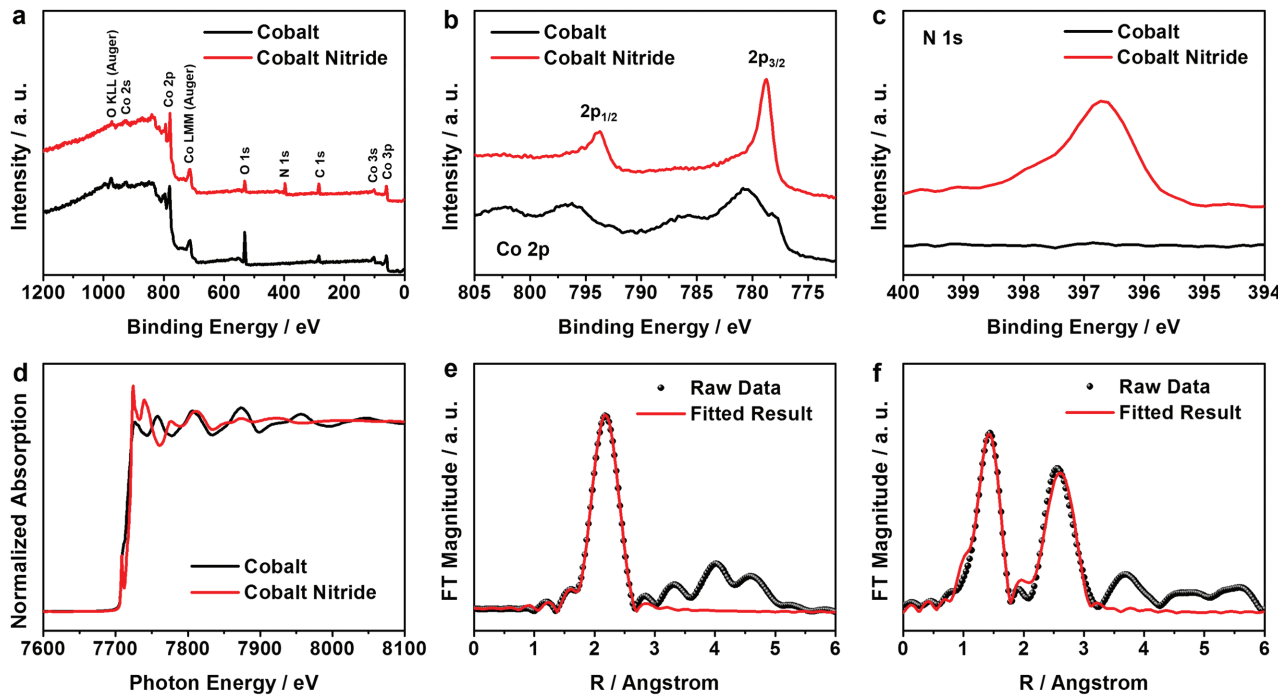


Figure 3. X-ray analyses. XPS a) survey, b) Co 2p, and c) N 1s spectra of the Co and the CoN films. d) The Co K-edge XANES spectra of the Co and the CoN films. e,f) The k^3 -weighted Fourier transforms of the EXAFS spectra at the Co K-edge for the (e) Co and (f) CoN films.

from the XRD analysis.^[67] Additionally, coordination numbers and bond lengths in the CoN film were obtained by extended X-ray absorption fine structure (EXAFS) analysis. Figure 3e,f shows the Fourier transformed k^3 -weighted EXAFS spectra of the Co and CoN deposited on FTO substrates. The fittings were performed by using Kaiser–Bessel function with $dk = 0.5$ and $dR = 0.5$, and the R -factors for the Co and CoN films were 0.0020 and 0.0032, respectively. In the Co film, Co–Co bond length was 2.490 Å, based on the assumption that the film was bulk Co with coordination number of 12. However, the Co–Co interatomic distance in the CoN film was 3.040 Å, which is a significantly larger value compared to the case of the Co, and the coordination number was 11.1. On the other hand, the calculated Co–N bond length was 1.862 Å, with the coordination number of 2.95. From the elongated Co–Co distance in the CoN film and clear observation of Co–N, it could be verified that complete nitridation of Co was achieved by the room-temperature vapor deposition in an inert condition.

2.2. Cobalt Nitride Nanofilms as Electrocatalytic Counter Electrodes of Dye-Sensitized Solar Cells

For the application of the CoN films as a low-cost counter electrode in DSCs (Figure 4a), cyclic voltammetry (CV) analyses were performed in order to evaluate electrocatalytic activity of the CoN film in I_3^-/I^- redox reactions. For comparison, the state-of-the-art Pt electrode was also prepared by thermal decomposition of H_2PtCl_6 on FTO substrate (hereafter denoted as Pt/FTO). Characterizations of the Pt electrode were carried out by SEM and XRD analyses, which are, respectively, displayed in Figures S2 and S3, Supporting Information). Figure 4b,c shows

the CV diagrams of Pt/FTO and the CoN electrodes in iodide redox electrolyte. There were two redox peaks clearly apparent in both directions of the potential sweep; one pair at higher potential correspond to the redox reaction of I_3^-/I_2 , and the other pair at lower potential are the signals from that of I_3^-/I^- .^[68] Given that the counter electrode serves as an electrocatalyst for the triiodide-to-iodide reaction ($I_3^- + 2e^- \rightarrow 3I^-$) in DSCs,^[69] the reduction currents that are apparent at the relatively low potential is a key indicator for the catalytic activity. Compared to the case of Pt/FTO, where sharp increase of the I_3^-/I^- current with a clear peak was observed after the onset, the CoN film exhibited a slightly larger overpotential. Though this observation implies that the CoN is less active than Pt, a large current density without a significant increase in overpotential clearly demonstrates that the CoN film is an effective electrocatalyst for iodide redox species.

DSCs were prepared by using N719-sensitized TiO_2 photoanodes and acetonitrile-based I_3^-/I^- redox electrolyte. Figure 4d shows the J – V curves of the DSCs employing Pt/FTO and the CoN as counter electrodes measured at the standard AM 1.5G condition. The parameters obtained from the J – V curves, namely, open-circuit voltage (V_{oc}), short-circuit current density (J_{sc}), fill factor (FF), and power conversion efficiency (η), are displayed in Table 1. The performance of the CoN was comparable to that of Pt/FTO in DSCs, manifesting η of 7.31% ($7.17 \pm 0.15\%$) while that of the conventional Pt-based DSC was 7.55% ($7.31 \pm 0.25\%$). It was directly confirmed from the actual devices that the CoN film is a promising candidate to replace costly Pt. The incident photon-to-current efficiency (IPCE) spectra of the DSCs are displayed in Figure 4e, and the IPCE matched well with the J – V results. Additional applications of the CoN nanofilms were carried out on DSCs

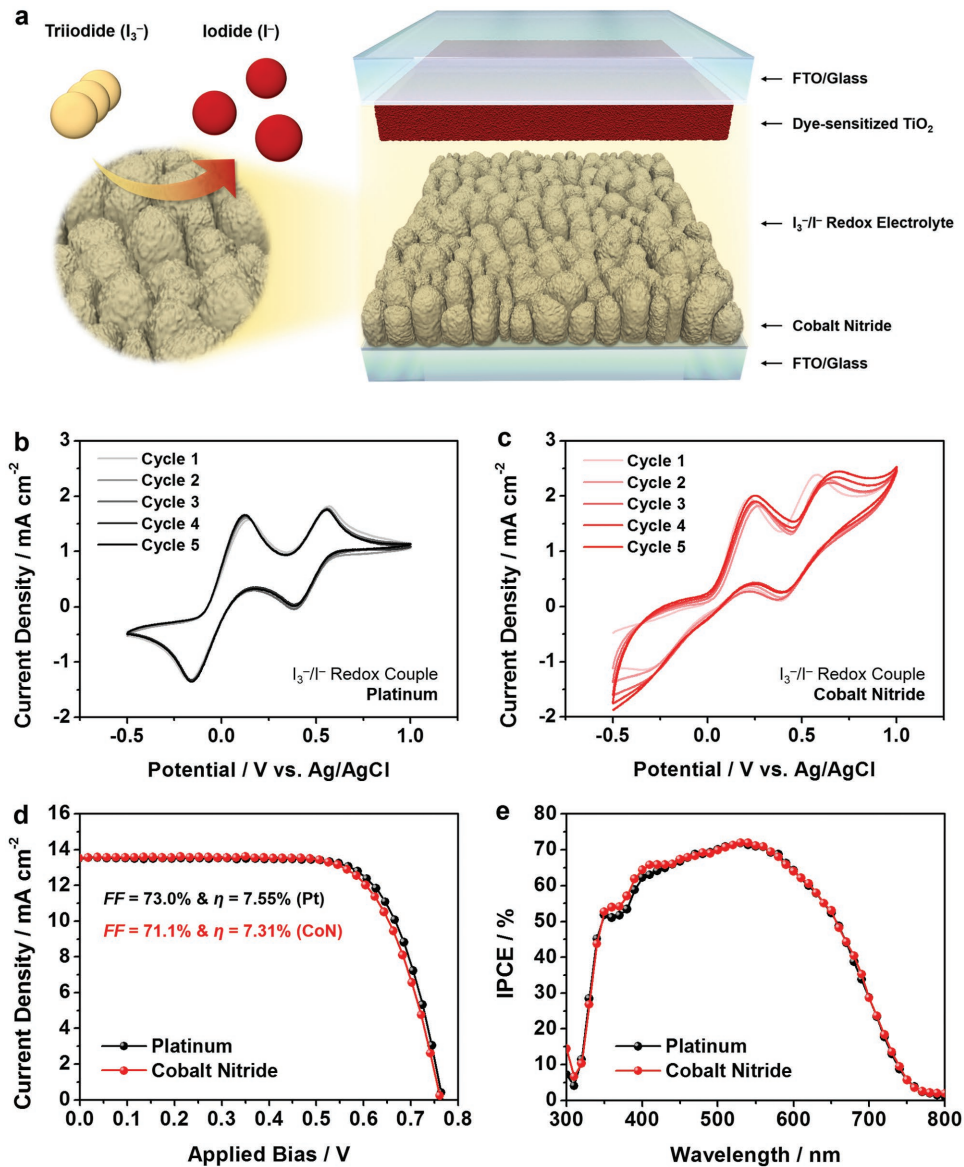


Figure 4. Application of the CoN film in dye-sensitized solar cells. a) A schematic illustration of a DSC employing the CoN film as the counter electrode which catalyzes electrochemical reduction of triiodides. CV diagrams of the b) Pt/FTO and c) CoN film. d) $J-V$ characteristics and e) IPCE spectra of DSCs employing the Pt/FTO and the CoN film as counter electrodes.

and QDSCs employing cobalt bipyridine and polysulfide redox electrolytes, respectively, and the results are summarized in a separate section in the Supporting Information (Tables S1 and S2, Figures S4–S8, Supporting Information).

Table 1. Summary of $J-V$ characteristics of DSCs employing the Pt/FTO and the CoN film as counter electrodes.

| | V_{oc} [V] | J_{sc} [mA cm^{-2}] | FF [%] | η [%] |
|----------------------|---------------------|----------------------------------|------------------|-------------------|
| Platinum | 0.766 | 13.5 | 73.0 | 7.55 |
| (Average \pm S.D.) | (0.759 ± 0.011) | (13.2 ± 0.5) | (73.0 ± 1.4) | (7.31 ± 0.25) |
| Cobalt nitride | 0.762 | 13.5 | 71.1 | 7.31 |
| (Average \pm S.D.) | (0.759 ± 0.004) | (13.2 ± 0.4) | (71.6 ± 0.6) | (7.17 ± 0.15) |

Since the vapor deposition of the CoN films was carried out at room temperature and in an inert condition, flexible CoN films were prepared by using indium tin oxide (ITO)/polyethylenenaphthalate (PEN) substrates. Pt-sputtered ITO/PEN was also prepared for comparison, because the thermal decomposition method damages ITO/PEN substrates. Figure S9 (Supporting Information) shows the digital photograph images of the Pt-deposited ITO/PEN (Pt/ITO/PEN) and the CoN-deposited ITO/PEN (CoN/ITO/PEN) that are highly flexible. As schematically depicted in Figure 5a, flexible DSCs were prepared by using the previously reported TiO_2 nanogel, which enables the sintering of TiO_2 nanoparticles at a mild temperature (below 200 °C).^[70,71] Though the overall performance of the DSCs was

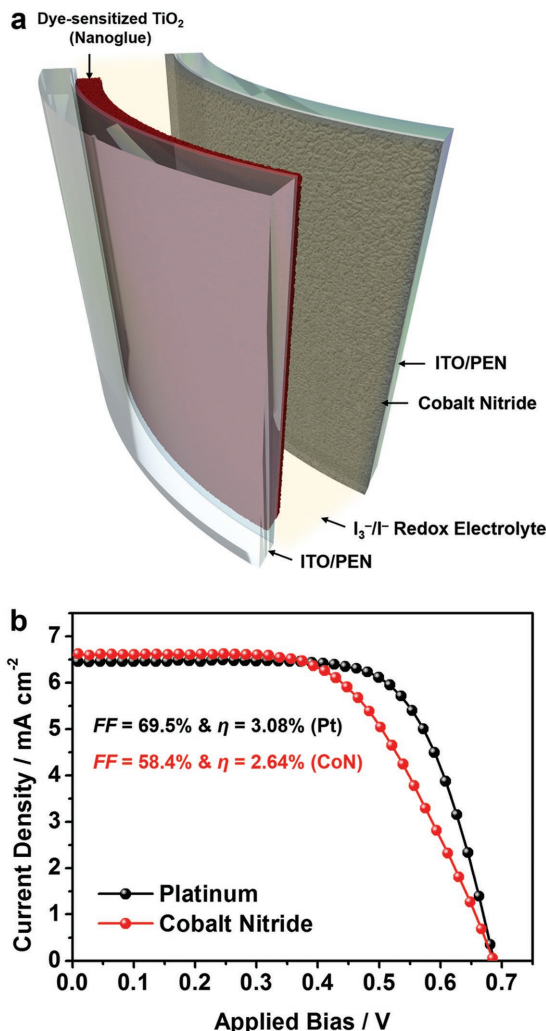


Figure 5. Application in flexible dye-sensitized solar cells. a) A schematic illustration of a flexible DSC comprising the TiO₂ nanoglue and the CoN film as a photoanode and a counter electrode, respectively. b) J–V characteristics of the flexible DSCs employing Pt and CoN deposited on ITO/PEN substrates as counter electrodes.

significantly lower than the rigid DSCs (owing to the usage of different type of photoanode), both of the flexible counter electrodes manifested reliable performance, as can be seen from the J–V curves in Figure 5b (see the summary of J–V parameters in Table S3, Supporting Information). Though there were negligible gaps in V_{oc} and J_{sc} , η was lower in the case of the CoN (2.64%) compared to the Pt-based counterpart (3.08%) due to the significant decrease in FF, which is ascribable to the difference in morphologies of the CoN/ITO/PEN from the CoN film deposited on FTO/glass. The SEM image of the CoN/ITO/PEN (Figure S10, Supporting Information) shows that the flexible CoN film has higher degree of flatness than those prepared on FTO/glass substrates, and this structural characteristic can be attributed to the diverse surface morphology of FTO/glass and ITO/PEN substrates (see SEM images in Figures S11 and S12, Supporting Information). Meanwhile, Pt-sputtered ITO/PEN has rice-like nanostructure (Figure S13, Supporting Informa-

tion) that is favorable for the electrocatalytic reactions regarding the number of active sites and mass transport of redox species in the electrolyte. Therefore, gap between the FFs of the Pt- and the CoN-based DSCs was increased in the flexible DSCs when compared with the DSCs employing rigid FTO/glass. However, feasibility of room-temperature vapor-deposited CoN for applications in flexible solar cells is strongly demonstrated from this investigation, and further enhancement in performance of the flexible CoN electrode is expected via proper structural optimizations.

2.3. Cobalt Nitride Nanofilm as a Hole Transport Layer in Inverted Planar Perovskite Solar Cells

In order to utilize the CoN film as a HTL in inverted planar PSCs, room-temperature vapor deposition of Co in an N₂-filled chamber was carried out onto ITO/glass substrates (see schematic illustration of a CoN film in Figure 6a). Extremely thin CoN films with high transparency were prepared by a shortened deposition time, and the prepared CoN films were utilized as a HTL for PSCs (see schematic illustration in Figure 6b). The work function of the CoN film was calculated as 3.9 eV from the ultraviolet photoelectron spectroscopy (UPS) valence band spectrum (Figure S14, Supporting Information). The energy level diagram of a PSC employing the CoN HTL (Figure 6b) shows that the energy level of the CoN film is located far from the valence band edge position (5.4 eV) of the methyl ammonium lead halide perovskite (CH₃NH₃PbI₃, hereafter denoted as MAPbI₃) light absorber. However, increase in work function was expected for the CoN due to inevitable surface oxidation of the CoN induced by direct contact with air or during the UV–ozone treatment (for a good adhesion between the CoN film and MAPbI₃), leading to a more favorable energy level for charge carrier transfer at the CoN/MAPbI₃ interface as a consequence.^[72,73] Since the uniformity and flatness of the HTL layer are the important requirements for high-performance inverted planar PSCs,^[74,75] the surface structure of the CoN film was first characterized by an atomic force microscope (AFM) and SEM. Figure 7a shows the AFM image of the CoN film, of which root-mean-square (RMS) roughness at the surface was measured as 1.5 nm. The morphology of the CoN film was additionally characterized by SEM (Figure 7b), and the high uniformity and flatness of the CoN film was verified. The morphology of the CoN film was almost identical to that of an ITO/glass substrate (Figure S15, Supporting Information), indicating the extremely small thickness of the CoN film.

MAPbI₃ layer was deposited on the CoN film by the Lewis-base adduct method,^[76] and the morphology and the crystalline property of the perovskite film was characterized by SEM and XRD analyses. From the top-view SEM image of the MAPbI₃/CoN/ITO/glass film displayed in Figure 7c, highly uniform perovskite film with large grains was observed. In order to prepare PSCs based on the CoN HTL, C₆₀/BCP layer was deposited onto the MAPbI₃ as an electron transport layer (ETL) followed by LiF/Al on the top as described in Figure 6b. Figure 7d shows the cross-sectional SEM image of a PSC employing the CoN film as a HTL. Around 20 nm thick CoN film was observable in between the ITO and the MAPbI₃ layer, and the conformal

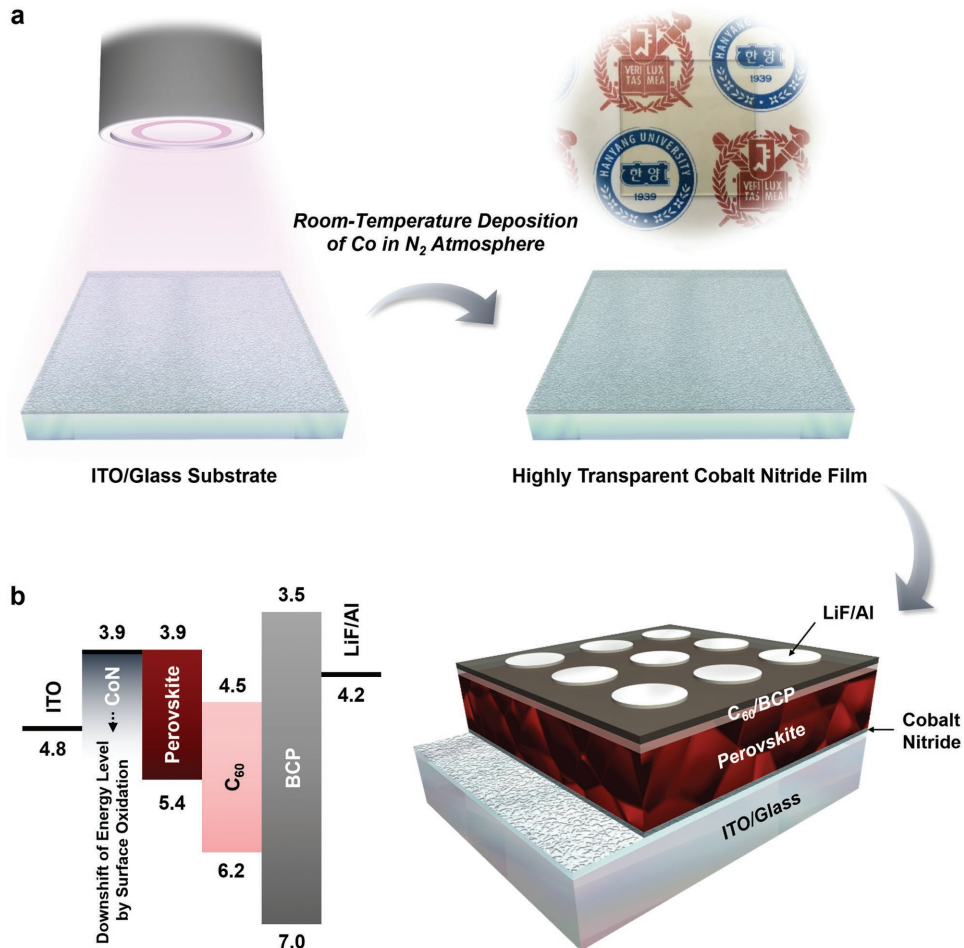


Figure 6. Preparation of the CoN films for perovskite solar cell applications. a) Schematic images illustrating the preparation of the transparent CoN film. b) An illustration depicting an inverted planar PSC employing the CoN film as a HTL and a schematic energy level diagram for the PSC. The energy levels are presented with regard to the vacuum level.

heterojunctions above the CoN HTL were also noted. Comparative investigations were additionally performed based on a conventional poly(3,4-ethylenedioxythiophene):poly(styrenesulfonate) (PEDOT:PSS) HTL (Figure S16, Supporting Information), and it could be concluded that the uniformity and crystallinity of the MAPbI₃ formed on the CoN film were in a comparable level to that on the PEDOT:PSS HTL.

The performance of the PSCs employing the CoN HTL was characterized in standard AM 1.5G condition, and the J-V characteristics obtained by forward and backward scans and the IPCE spectra are displayed in Figure 7e and f, respectively. The η of the PSC employing the CoN film appeared as $14.3 \pm 0.5\%$ and reached up to 15.0% in the reverse scan of the best performing cell (detailed J-V parameters are displayed in Table 2). Though the overall cell performance was inferior to the PEDOT:PSS HTL-based PSCs prepared by the same method, mainly due to a relatively low transparency of the CoN film (Table S4 and Figures S17–S19, Supporting Information), the CoN-based PSCs show excellent performance among state-of-the-art PSCs employing inorganic HTLs (see Table S5, Supporting Information). In addition, PSCs with the CoN HTL manifest high stability and reliability in operations under light-soaking conditions (Figure S20,

Supporting Information), verifying the desirable feasibility of the CoN for use in PSCs. Additionally, it is notable to observe that the V_{oc} is larger in the CoN-based PSCs (1.01 ± 0.01 V) when compared with the cases of other inorganic HTLs (Table S5, Supporting Information) or even with that of PEDOT:PSS prepared by using the same procedure.

In order to understand the charge transfer dynamics in the CoN HTL, photoluminescence (PL) and electrochemical impedance spectroscopy (EIS) measurements were performed, and the results were compared with those obtained from the PEDOT:PSS counterpart. Figure 8a shows the steady-state PL spectra of MAPbI₃/HTL/ITO/glass wherein the CoN film and PEDOT:PSS were used as the HTLs. From the significantly larger PL intensity for the CoN-based perovskite film, it was clear that the charge extraction property of the CoN was inferior to that of PEDOT:PSS. In addition, time-resolved PL decay measurements were also carried out for a quantitative comparison on the charge extraction (Figure 8b). The PL decay curves were fitted according to the following third-order exponential decay model^[77]

$$\gamma(t) = \gamma_0 + A_1 e^{-t/\tau_1} + A_2 e^{-t/\tau_2} + A_3 e^{-t/\tau_3} \quad (1)$$

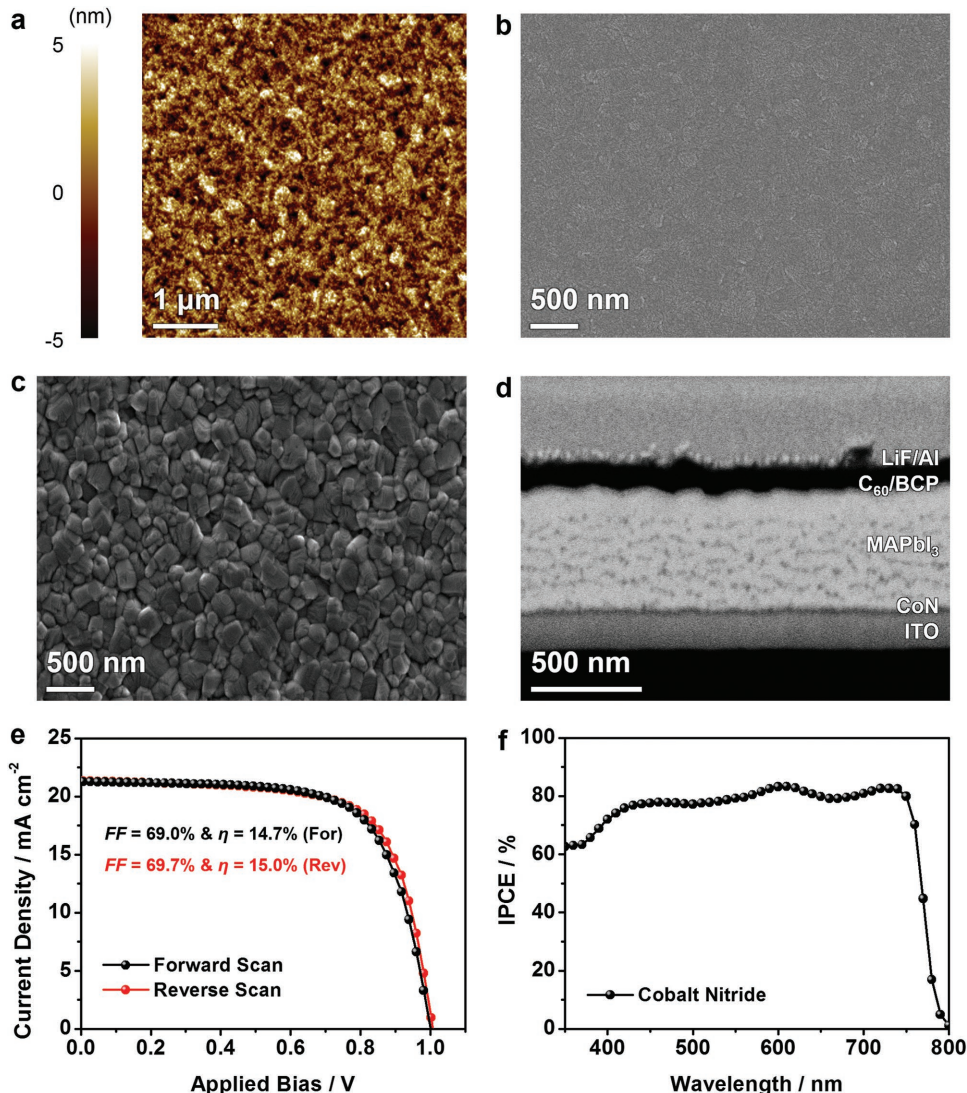


Figure 7. Perovskite solar cells employing the cobalt nitride hole transport layer. a) AFM topography image ($5 \mu\text{m} \times 5 \mu\text{m}$) of the CoN film on ITO/glass. The RMS roughness of the CoN film obtained from the AFM analysis was 1.5 nm. Top-view SEM images of the b) CoN film and c) MAPbI₃ deposited on the CoN. d) Cross-sectional SEM image of a PSC employing the CoN as a HTL. e) J - V characteristics and f) IPCE spectrum of the PSC with the CoN film as a HTL.

Among the parameters in the decay model, τ_1 is the fast decay component term that shows the kinetics of charge extraction. The τ_1 values obtained from the CoN and PEDOT:PSS were 9.60 and 2.67 ns, respectively, showing that the charge extraction at the MAPbI₃/HTL interface is significantly faster in the case of PEDOT:PSS compared to the CoN. The detailed fitting results for other constants are summarized in Table S6 (Supporting Information).

Table 2. Summary of J - V characteristics of PSCs employing the CoN film as HTLs.

| | V_{oc} [V] | J_{sc} [mA cm^{-2}] | FF [%] | η [%] |
|----------------------|---------------------|----------------------------------|--------------------|--------------------|
| Forward scan | 1.00 | 21.3 | 69.0 | 14.7 |
| Reverse scan | 1.01 | 21.3 | 69.7 | 15.0 |
| (Average \pm S.D.) | (1.01 ± 0.01) | (20.6 ± 0.7) | (68.7 ± 1.5) | (14.3 ± 0.5) |

Figure 8c–e shows the fitted results of the EIS data of the PSCs employing the CoN or PEDOT:PSS as HTLs. Full Nyquist spectra and the equivalent circuit are depicted in Figure S21 (Supporting Information), and the detailed values are summarized in Table S7 (Supporting Information). Series resistance (R_s), which shows the ohmic properties of the PSCs, appeared to be similar in both cases (Figure 8c). In contrast, significant differences were observable in charge transfer resistance (R_{ct} , Figure 8d) and recombination resistance (R_{rec} , Figure 8e). The CoN manifested a larger R_{ct} at MAPbI₃/HTL interface compared to PEDOT:PSS, and these results matched well with the observations in PL analyses. In the meantime, it was notable that the R_{rec} was larger in the PSC with the CoN HTL than that with PEDOT:PSS, even exhibiting nearly an order of magnitude higher R_{rec} values at the voltage range of 0.4–0.6 V. This

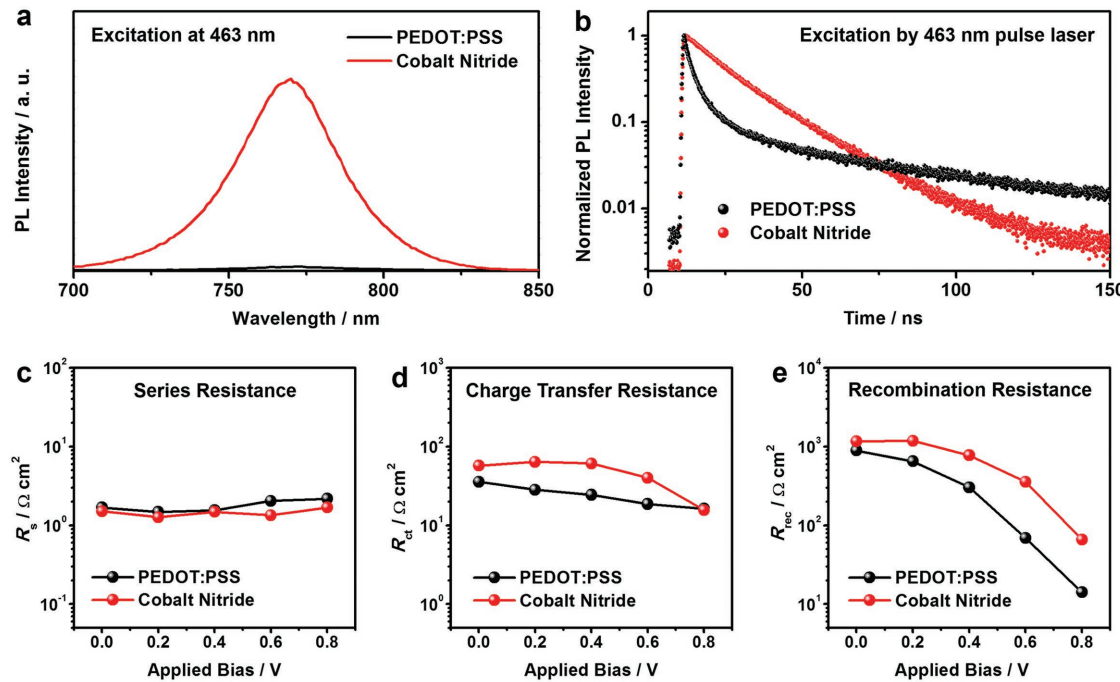


Figure 8. Charge transfer kinetics in perovskite solar cells. a) Steady-state PL spectra and b) time-resolved PL spectra of perovskite films deposited on PEDOT:PSS and the CoN HTLs by excitation at 463 nm. c) Series resistance, d) charge transfer resistance, and e) recombination resistance obtained by fitting the EIS results displayed in Figure S21 (Supporting Information).

difference implies that charge recombination is preferably suppressed in the PSCs employing the CoN HTL compared to the PEDOT:PSS-based PSCs, and this is accountable for the higher V_{oc} of 1.01 V in CoN-based cells. Meanwhile, it is clear from the $J-V$ curves that the FF is higher in the case of PEDOT:PSS compared to the CoN case, though suppression of charge recombinations was superior in PSCs employing the CoN HTL. According to the previous report by Juarez-Perez et al., the sum of R_s and R_{ct} represents the overall resistance during the operation of PSCs and has dominant influence on the FF.^[78] Our results are in accordance with the previous observation, given that the $R_s + R_{ct}$ is larger for the CoN-based PSCs when compared with PEDOT:PSS-based cells.

Finally, the CoN was deposited on the flexible ITO/PEN substrate, and flexible PSCs were prepared as schematically described in Figure 9a (see SEM images in Figure S22, Supporting Information). The η of 10.2% calculated from the $J-V$ characteristic displayed in Figure 9b shows the high feasibility of the CoN film for use in HTL for flexible PSCs (see Table S8, Supporting Information, for detailed $J-V$ parameters), while the performance of the cell was inferior to the rigid counterpart. Since the CoN is an inorganic polycrystalline film, it is vulnerable to mechanical deformations, and this is clear from the smaller degree of performance drop when polymeric PEDOT:PSS was used as an HTL for flexible PSCs (32.0% drop for CoN compared with 13.7% drop for PEDOT:PSS, see

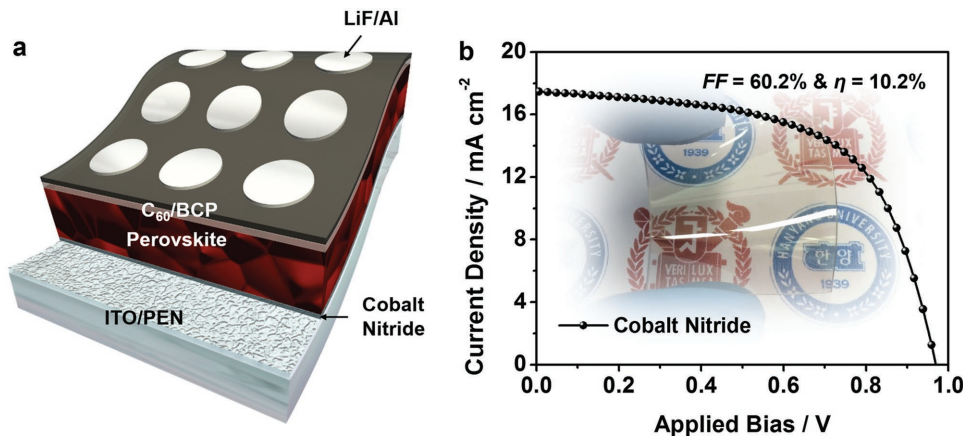


Figure 9. Application in flexible perovskite solar cells. a) A schematic illustration and b) $J-V$ characteristic of a flexible PSC comprising the CoN film deposited on a flexible ITO/PEN film as the HTL.

Table S9 and Figure S23, Supporting Information). Nevertheless, this result still demonstrates that the CoN is a highly promising HTL for PSCs with wide room for further modifications, possibly considered for applications requiring flexibility (such as wearable electronic devices) after proper optimizations such as incorporation of flexible conducting agents.

3. Conclusions

In this study, CoN nanofilms were prepared by room-temperature vapor deposition of Co in an inert N₂ atmosphere. The CoN film in DSCs manifested a high performance similar to the conventional Pt electrode, and when the CoN was used as a HTL in PSCs, power conversion efficiency up to 15.0%, which is comparable to those of state-of-the-art PSCs based on inorganic HTLs, was achieved. Furthermore, feasibilities of the CoN for flexible solar cell applications were verified in both DSCs and PSCs, demonstrating the advantages of the facile room-temperature fabrication procedure and wide range of potential applications. Considering the economic advantage of the CoN for DSCs and high performance obtained in CoN-based PSCs even though this work is the first demonstration of the nitride hole transport materials according to the best of our knowledge, the strategies and observations in the present study are anticipated to provide new insights not only to the development of low-cost electrode materials but also to the process designs in view of industrial and practical applications.

4. Experimental Section

Preparation of the Cobalt Nitride Nanofilms: The CoN nanofilms were fabricated by a radio frequency sputtering of cobalt at the power of 300 W and 13.56 MHz frequency in a chamber filled with 80 mTorr of N₂ gas. The deposition processes were carried out in room temperature, and the substrate temperature was 25 °C. For mesoscopic solar cells, the deposition was carried out onto FTO/glass substrates for 8 h, and deposition time was shortened to 20 min for the preparation of the CoN film on ITO/glass substrates for PSCs. Flexible ITO/PEN substrates were used for the investigations on the flexible solar cell applications.

Preparation of Mesoscopic Solar Cells: All of the chemical reagents were purchased from Sigma-Aldrich and used without further purification (otherwise stated in the text). The iodide redox electrolyte for CV analysis was prepared by mixing 10 × 10⁻³ M LiI, 1 × 10⁻³ M I₂, 0.1 × 10⁻³ M LiClO₄ in acetonitrile, and that for the DSCs was composed of 0.6 M 1-butyl-3-methylimidazolium iodide, 30 × 10⁻³ M I₂, 0.1 M guanidinium thiocyanate, and 0.5 M 4-tert-butylpyridine in a mixture of acetonitrile and valeronitrile (volumetric ratio = 85:15). The TiO₂ photoanode was fabricated by a conventional method; TiO₂ paste containing ≈20 nm sized nanoparticles was prepared via the method in a previous report,^[79] and the paste was cast on a FTO/glass substrate by doctor blading. Then the electrode was sintered at 500 °C in air for 30 min, and TiCl₄ post-treatment was performed in order to increase the roughness factor and enhance the electron injection from sensitizers to the TiO₂ conduction band.^[80] Dye molecules were chemisorbed on the TiO₂ surface by immersing the electrode in ethanolic solution containing 0.5 × 10⁻³ M N719 (Ru 535-bisTBA, Solaronix) for 24 h. For the cell assembly, photoanodes and counter electrodes were attached by using a thermoplastic sealant (Surlyn, Dupont). The electrolytes were injected into the cell through the pre-drilled holes.

Preparation of Perovskite Solar Cells: CoN nanofilms prepared on ITO/glass substrates were treated with UV-ozone for 20 min prior to coating of perovskite layer. MAPbI₃ perovskite layer was fabricated through Lewis base adduct method reported previously.^[76] PbI₂ (Alfa Aesar),

methylammonium iodide (MAI) (Xi'an Polymer Light Tech. Corp.), and dimethyl sulfoxide (DMSO) were dissolved into dimethylformamide (DMF) with molar ratio of 1:1:1 at 50 wt%. 35 μL of the precursor solution was spin-coated onto the CoN film at 4000 rpm for 20 s. During the spin-coating process, 0.3 mL of diethyl ether was vigorously cast onto the substrate to obtain a yellow transparent film. Then, a two-step annealing process (65 °C for 1 min and 100 °C for 4 min) was carried out. During the annealing process, the transparent film changed into a dark-brown perovskite film. After the formation of the perovskite layer, the substrates were transferred to a vacuum thermal evaporator. C₆₀ (20 nm), BCP (10 nm), LiF (0.5 nm), and Al (120 nm) were deposited under pressure of <10⁻⁷ bar.

Physical and Electrochemical Characterizations: XRD measurements were performed using Rigaku D-MAX2500-PC, and XPS spectra were obtained by Thermo SIGMA PROBE. SEM and TEM analyses were, respectively, performed using Carl Zeiss AURIGA and FEI Tecnai F20. Surface morphology measurement of HTL films was conducted with atomic force microscopy (Park Systems NX10). XAFS analyses were carried out by synchrotron measurement at 8C beamline of Pohang Accelerator Laboratory (PAL) in fluorescence mode. CV analyses were performed in a three-electrode system comprising a Pt mesh (counter electrode) and an Ag/AgCl (saturated KCl) reference electrode using a potentiostat (Metrohm Autolab PGSTAT128N). Photoluminescence measurement was implemented using a spectrofluorometer (Horiba Scientific FluoroMax-4) with 463 nm excitation laser. EIS measurements were carried out using a potentiostat (CHI 600D, CH Instruments). The performance of the solar cells was measured in the standard AM 1.5G condition by using a solar simulator equipped with a 1600 W xenon lamp (Yamashita Denso YSS-200A). IPCEs were measured by using a 75 W xenon lamp and a monochromator at short-circuit condition.

Supporting Information

Supporting Information is available from the Wiley Online Library or from the author.

Acknowledgements

J.S.K., J.-Y.K., and J.Y. contributed equally to this work. This work was supported by the Institute for Basic Science (IBS-R006-G1 and IBS-R006-D1) in Republic of Korea and the Global Frontier R&D Program on Center for Multiscale Energy System (2012M3A6A7054855 and 2012M3A6A7054856) funded by the National Research Foundation under the Ministry of Science, ICT & Future Planning, Republic of Korea. This research was also supported by Basic Science Research Program (2017R1D1A1B03035077) through the National Research Foundation of Korea (NRF) funded by the Ministry of Education, Republic of Korea.

Conflict of Interest

The authors declare no conflict of interest.

Keywords

cobalt nitride, counter electrodes, dye-sensitized solar cells, hole transport materials, perovskite solar cells

Received: November 8, 2017

Revised: December 6, 2017

Published online:

- [1] M. Graetzel, R. A. Janssen, D. B. Mitzi, E. H. Sargent, *Nature* **2012**, *488*, 304.
- [2] B. E. Hardin, H. J. Snaith, M. D. McGehee, *Nat. Photonics* **2012**, *6*, 162.
- [3] T. M. Brenner, D. A. Egger, L. Kronik, G. Hodes, D. Cahen, *Nat. Rev. Mater.* **2016**, *1*, 15007.
- [4] N. S. Lewis, *Science* **2016**, *351*, aad5117.
- [5] B. O'Regan, M. Grätzel, *Nature* **1991**, *353*, 737.
- [6] A. Hagfeldt, G. Boschloo, L. Sun, L. Kloo, H. Pettersson, *Chem. Rev.* **2010**, *110*, 6595.
- [7] A. Yella, H.-W. Lee, H. N. Tsao, C. Yi, A. K. Chandiran, M. K. Nazeeruddin, E. W.-G. Diau, C.-Y. Yeh, S. M. Zakeeruddin, M. Grätzel, *Science* **2011**, *334*, 629.
- [8] M. Ye, X. Wen, M. Wang, J. Iocozzia, N. Zhang, C. Lin, Z. Lin, *Mater. Today* **2015**, *18*, 155.
- [9] M. Freitag, J. Teuscher, Y. Saygili, X. Zhang, F. Giordano, P. Liska, J. Hua, S. M. Zakeeruddin, J.-E. Moser, M. Grätzel, A. Hagfeldt, *Nat. Photonics* **2017**, *11*, 372.
- [10] H.-S. Kim, C.-R. Lee, J.-H. Im, K.-B. Lee, T. Moehl, A. Marchioro, S.-J. Moon, R. Humphry-Baker, J.-H. Yum, J. E. Moser, M. Grätzel, N.-G. Park, *Sci. Rep.* **2012**, *2*, 591.
- [11] M. M. Lee, J. Teuscher, T. Miyasaka, T. N. Murakami, H. J. Snaith, *Science* **2012**, *338*, 643.
- [12] J. Burschka, N. Pellet, S.-J. Moon, R. Humphry-Baker, P. Gao, M. K. Nazeeruddin, M. Grätzel, *Nature* **2013**, *499*, 316.
- [13] W. S. Yang, J. H. Noh, N. J. Jeon, Y. C. Kim, S. Ryu, J. Seo, S. I. Seok, *Science* **2015**, *348*, 1234.
- [14] D. Bi, C. Yi, J. Luo, J.-D. Décoppet, F. Zhang, S. M. Zakeeruddin, X. Li, A. Hagfeldt, M. Grätzel, *Nat. Energy* **2016**, *1*, 16142.
- [15] W. S. Yang, B.-W. Park, E. H. Jung, N. J. Jeon, Y. C. Kim, D. U. Lee, S. S. Shin, J. Seo, E. K. Kim, J. H. Noh, S. I. Seok, *Science* **2017**, *356*, 1376.
- [16] S. Matthew, A. Yella, P. Gao, R. Humphry-Baker, B. F. E. Curchod, N. Ashari-Astani, I. Tavernelli, U. Rothlisberger, M. K. Nazeeruddin, M. Grätzel, *Nat. Chem.* **2014**, *6*, 242.
- [17] Y. Liu, R. Che, G. Chen, J. Fan, Z. Sun, Z. Wu, M. Wang, B. Li, J. Wei, Y. Wei, G. Wang, G. Guan, A. A. Elzatahry, A. A. Bagabas, A. M. Al-Enizi, Y. Deng, H. Peng, D. Zhao, *Sci. Adv.* **2015**, *1*, e1500166.
- [18] K. Kakiage, Y. Aoyama, T. Yano, K. Oya, J.-i. Fujisawa, M. Hanaya, *Chem. Commun.* **2015**, *51*, 15894.
- [19] S. Jang, J. S. Kang, J.-K. Lee, S. M. Kim, Y. J. Son, A. Lim, H. Cho, J. Kim, J. Jeong, G. Lee, Y.-E. Sung, M. Choi, *Adv. Funct. Mater.* **2016**, *26*, 6584.
- [20] N. J. Jeon, J. H. Noh, Y. C. Kim, W. S. Yang, S. Ryu, S. I. Seok, *Nat. Mater.* **2014**, *13*, 897.
- [21] J.-H. Im, I.-H. Jang, N. Pellet, M. Grätzel, N.-G. Park, *Nat. Nanotechnol.* **2014**, *9*, 927.
- [22] H. S. Jung, N.-G. Park, *Small* **2015**, *11*, 10.
- [23] M. Saliba, T. Matsui, K. Domanski, J.-Y. Seo, A. Ummadisingu, S. M. Zakeeruddin, J.-P. Correa-Baena, W. R. Tress, A. Abate, A. Hagfeldt, M. Grätzel, *Science* **2016**, *354*, 206.
- [24] Y. H. Park, I. Jeong, S. Bae, H. J. Son, P. Lee, J. Lee, C.-H. Lee, M. J. Ko, *Adv. Funct. Mater.* **2017**, *27*, 1605988.
- [25] J. Yoon, H. Sung, G. Lee, W. Cho, N. Ahn, H. S. Jung, M. Choi, *Energy Environ. Sci.* **2017**, *10*, 337.
- [26] S. S. Shin, E. J. Yeom, W. S. Yang, S. Hur, M. G. Kim, J. Im, J. Seo, J. H. Noh, S. I. Seok, *Science* **2017**, *356*, 167.
- [27] N.-G. Park, M. Grätzel, T. Miyasaka, K. Zhu, K. Emery, *Nat. Energy* **2016**, *1*, 16152.
- [28] M. Wu, X. Lin, Y. Wang, L. Wang, W. Guo, D. Qi, X. Peng, A. Hagfeldt, M. Grätzel, T. Ma, *J. Am. Chem. Soc.* **2012**, *134*, 3419.
- [29] Y. Zhu, H. Guo, H. Zheng, Y.-N. Lin, C. Gao, Q. Han, M. Wu, *Nano Energy* **2016**, *21*, 1.
- [30] S. Thomas, T. G. Deepak, G. S. Anjusree, T. A. Arun, S. V. Nair, A. S. Nair, *J. Mater. Chem. A* **2014**, *2*, 4474.
- [31] M. Kouhnnavard, N. A. Ludin, B. V. Ghaffari, K. Sopian, S. Ikeda, *ChemSusChem* **2015**, *8*, 1510.
- [32] L. Calió, S. Kazim, M. Grätzel, S. Ahmad, *Angew. Chem., Int. Ed.* **2016**, *55*, 14522.
- [33] Z. H. Bakr, Q. Wali, A. Fakharuddin, L. Schmidt-Mende, T. M. Brown, R. Jose, *Nano Energy* **2017**, *34*, 271.
- [34] M. Wu, X. Lin, A. Hagfeldt, T. Ma, *Angew. Chem., Int. Ed.* **2011**, *50*, 3520.
- [35] J. S. Kang, J. Kim, M. J. Lee, Y. J. Son, J. Jeong, D. Y. Chung, A. Lim, H. Choe, H. S. Park, Y.-E. Sung, *Nanoscale* **2017**, *9*, 5413.
- [36] Q. W. Jiang, G. R. Li, X. P. Gao, *Chem. Commun.* **2009**, 6720.
- [37] G. R. Li, J. Song, G. L. Pan, X. P. Gao, *Energy Environ. Sci.* **2011**, *4*, 1680.
- [38] S. H. Park, Y.-H. Cho, M. Choi, H. Choi, J. S. Kang, J. H. Um, J.-W. Choi, H. Choe, Y.-E. Sung, *Surf. Coat. Technol.* **2014**, *259*, 560.
- [39] M. Chen, L.-L. Shao, Z.-M. Gao, T.-Z. Ren, Z.-Y. Yuan, *J. Power Sources* **2015**, 286, 82.
- [40] Y. Hou, D. Wang, X. H. Yang, W. Q. Fang, B. Zhang, H. F. Wang, G. Z. Lu, P. Hu, H. J. Zhao, H. G. Yang, *Nat. Commun.* **2013**, *4*, 1583.
- [41] X. Zheng, J. Guo, Y. Shi, F. Xiong, W.-H. Zhang, T. Ma, C. Li, *Chem. Commun.* **2013**, *49*, 9645.
- [42] Y. Duan, Q. Tang, J. Liu, B. He, L. Yu, *Angew. Chem., Int. Ed.* **2014**, *53*, 14569.
- [43] M. Wu, Y.-n. Lin, H. Guo, T. Ma, A. Hagfeldt, *J. Power Sources* **2014**, *263*, 154.
- [44] Y. Zhu, H. Guo, H. Zheng, Y.-N. Lin, C. Gao, Q. Han, M. Wu, *Nano Energy* **2016**, *21*, 1.
- [45] Y. Zhu, C. Gao, Q. Han, Z. Wang, Y. Wang, H. Zheng, M. Wu, *J. Catal.* **2017**, *346*, 62.
- [46] J. A. Christians, R. C. M. Fung, P. V. Kamat, *J. Am. Chem. Soc.* **2014**, *136*, 758.
- [47] P. Qin, S. Tanaka, S. Ito, N. Tetreault, K. Manabe, H. Nishino, M. K. Nazeeruddin, M. Grätzel, *Nat. Commun.* **2014**, *5*, 3834.
- [48] S. Ye, W. Sun, Y. Li, W. Yan, H. Peng, Z. Bian, Z. Liu, C. Huang, *Nano Lett.* **2015**, *15*, 3723.
- [49] V. E. Madhavan, I. Zirmermann, C. Roldán-Carmona, G. Grancini, M. Buffiere, A. Belaïdi, M. K. Nazeeruddin, *ACS Energy Lett.* **2016**, *1*, 1112.
- [50] Z. Zhu, Y. Bai, T. Zhang, Z. Liu, X. Long, Z. Wei, Z. Wang, L. Zhang, J. Wang, F. Yan, S. Yang, *Angew. Chem., Int. Ed.* **2014**, *53*, 12571.
- [51] J. H. Park, J. Seo, S. Park, S. S. Shin, Y. C. Kim, N. J. Jeon, H.-W. Shin, T. K. Ahn, J. H. Noh, S. C. Yoon, C. S. Hwang, S. I. Seok, *Adv. Mater.* **2015**, *27*, 4013.
- [52] C. Zuo, L. Ding, *Small* **2015**, *11*, 5528.
- [53] M. Cheng, Y. Li, M. Safdari, C. Chen, P. Liu, L. Kloo, L. Sun, *Adv. Energy Mater.* **2017**, *7*, 1602556.
- [54] L. S. Khanzada, I. Levchuk, Y. Hou, H. Azimi, A. Osvet, R. Ahmad, M. Brandl, P. Herre, M. Distaso, R. Hock, W. Peukert, M. Batentschuk, C. J. Brabec, *Adv. Funct. Mater.* **2016**, *26*, 8300.
- [55] B. Koo, H. Jung, M. Park, J.-Y. Kim, H. J. Son, J. Cho, M. J. Ko, *Adv. Funct. Mater.* **2016**, *26*, 5400.
- [56] E. Furimsky, *Appl. Catal., A* **2003**, *240*, 1.
- [57] K. Xu, P. Chen, X. Li, Y. Tong, H. Ding, X. Wu, W. Chu, Z. Peng, C. Wu, Y. Xie, *J. Am. Chem. Soc.* **2015**, *137*, 4119.
- [58] P. Chen, K. Xu, Z. Fang, Y. Tong, J. Wu, X. Lu, X. Peng, H. Ding, C. Wi, Y. Xie, *Angew. Chem., Int. Ed.* **2015**, *54*, 14710.
- [59] M. Wu, Q. Zhang, J. Xiao, C. Ma, X. Lin, C. Miao, Y. He, Y. Gao, A. Hagfeldt, T. Ma, *J. Mater. Chem.* **2011**, *21*, 10761.
- [60] M. Wu, H. Guo, Y.-N. Lin, K. Wu, T. Ma, A. Hagfeldt, *J. Phys. Chem. C* **2014**, *118*, 12625.
- [61] A. A. Kodentsov, M. J. H. van Dal, C. Cserháti, L. Darócz, F. J. J. van Loo, *Acta. Mater.* **1999**, *47*, 3169.

- [62] S. Desmoulins-Krawiec, C. Aymonier, A. Loppinet-Serani, F. Weill, S. Gorsse, J. Etourneau, F. Cansell, *J. Mater. Chem.* **2004**, *14*, 228.
- [63] Q. W. Jiang, G. R. Li, S. Liu, X. P. Gao, *J. Phys. Chem. C* **2010**, *114*, 13397.
- [64] S. C. Petitto, M. A. Langell, *J. Vac. Sci. Technol., A* **2004**, *22*, 1690.
- [65] B. Varghese, T. C. Hoong, Z. Yanwu, M. V. Reddy, B. V. R. Chowdari, A. T. S. Wee, T. B. C. Vincent, C. T. Lim, C.-H. Sow, *Adv. Funct. Mater.* **2007**, *17*, 1932.
- [66] Z.-S. Wu, W. Ren, L. Wen, L. Gao, J. Zhao, Z. Chen, G. Zhou, F. Li, H.-M. Cheng, *ACS Nano* **2010**, *4*, 3187.
- [67] H. Modrow, S. Bucher, J. J. Rehr, A. L. Ankudinov, *Phys. Rev. B* **2003**, *67*, 035123.
- [68] J. D. Roy-Mayhew, D. J. Bozym, C. Punckt, I. A. Aksay, *ACS Nano* **2010**, *4*, 6203.
- [69] A. Hauch, A. Georg, *Electrochim. Acta* **2001**, *46*, 3457.
- [70] Y. Li, W. Lee, D.-K. Lee, K. Kim, N.-G. Park, M. J. Ko, *Appl. Phys. Lett.* **2011**, *98*, 103301.
- [71] Y. Li, K. Yoo, D.-K. Lee, J. Y. Kim, H. Kim, B. S. Kim, M. J. Ko, *Nanoscale* **2013**, *5*, 4711.
- [72] T. J. Chuang, C. R. Brundle, D. W. Rice, *Surf. Sci.* **1976**, *59*, 413.
- [73] M. T. Greiner, M. G. Helander, W.-M. Tang, Z.-B. Wang, J. Qiu, Z.-H. Lu, *Nat. Mater.* **2012**, *11*, 76.
- [74] N. S. Kang, M. H. Hoang, D. H. Choi, B.-K. Ju, J.-M. Hong, J.-W. Yu, *Macromol. Res.* **2013**, *21*, 65.
- [75] H. Sung, N. Ahn, M. S. Jang, J.-K. Lee, H. Yoon, N.-G. Park, M. Choi, *Adv. Energy Mater.* **2016**, *6*, 1501873.
- [76] N. Ahn, D.-Y. Son, I.-H. Jang, S. M. Kang, M. Choi, N.-G. Park, *J. Am. Chem. Soc.* **2015**, *137*, 8696.
- [77] M.-c. Kim, B. J. Kim, D.-Y. Son, N.-G. Park, H. S. Jung, M. Choi, *Nano Lett.* **2016**, *16*, 5756.
- [78] E. J. Juarez-Perez, M. Wußler, F. Fabregat-Santiago, K. Lakus-Wollny, E. Mankel, T. Mayer, W. Jaegermann, I. Mora-Sero, *J. Phys. Chem. Lett.* **2014**, *5*, 680.
- [79] H.-J. Koo, J. Park, B. Yoo, K. Yoo, K. Kim, N.-G. Park, *Inorg. Chim. Acta* **2008**, *361*, 677.
- [80] P. M. Sommeling, B. C. O'Regan, R. R. Haswell, H. J. P. Smit, N. J. Bakker, J. J. T. Smits, J. M. Kroon, J. A. M. Roosmalen, *J. Phys. Chem. B* **2006**, *110*, 19191.